Critical Size of a Nano SnO_2 Electrode for Li-Secondary Battery

Chunjoong Kim,[†] Mijung Noh,[‡] Myungsuk Choi,[†] Jaephil Cho,*[,‡] and Byungwoo Park*[,†]

School of Materials Science and Engineering, and Research Center for Energy Conversion and Storage, Seoul National University, Seoul, Korea, and Department of Applied Chemistry, Kumoh National Institute of Technology, Gumi, Korea

Received November 13, 2004. Revised Manuscript Received March 18, 2005

SnO_2 nanoparticles with different sizes of ∼3, ∼4, and ∼8 nm were synthesized using a hydrothermal method at 110, 150, and 200 °C, respectively. The results showed that the ∼3 nm-sized SnO_2 nanoparticles had a superior capacity and cycling stability as compared to the ∼4 and ∼8 nm-sized ones. The ∼3 nm-sized nanoparticles exhibited an initial capacity of 740 mAh/g with negligible capacity fading. The electrochemical properties of these nanoparticles were superior to those of thin-film analogues. Transmission electron microscopy (TEM) and X-ray diffraction (XRD) confirmed that the ∼3 nm-sized SnO_2 nanoparticles after electrochemical tests did not aggregate into larger Sn clusters, in contrast to those observed with the ∼4 and ∼8 nm-sized ones.

Introduction

Many efforts have been made to implant a Sn-based anode into a Li-secondary battery since it was first reported by Idota et al. in 1997.[1] These electrodes exhibited a higher capacity (>600 mAh/g) than the conventional graphite anode (372 mAh/g), but showed faster capacity fading upon cycling. Coutney et al. rationalized the reaction of SnO_2 with lithium, by $SnO_2 + 4Li \rightarrow Sn + 2Li_2O$ and $Sn + xLi \leftrightarrow Li_xSn$.[2] The maximum theoretical capacity of the SnO_2 anode is 781 mAh/g by this mechanism. The irreversible initial capacity loss is due to the formation of amorphous Li_2O matrix. The most detrimental factor that hinders the use of a SnO_2 anode in Li-ion cells is its poor cycling stability as a result of the drastic volume change between Sn and $Li_{4.4}Sn$ of 358%.[3] Consequently, the particles become detached and electrically inactive. Diffraction studies confirmed that the small and active Sn particles aggregated into larger and inactive Sn clusters during cycling.[4]

Several methods have been proposed to minimize such a drastic volume change. Li et al. reported that SnO_2 nanofibers effectively accommodated the volume change.[5] This anode material retained a good cycling stability at a high charge rate. Thin-film SnO_2 was also studied for the same purpose.[6,7] However, these electrodes were not economically feasible for Li-ion cells. $M_xSn_yO_z$ compounds were also reported,[8−13] where M (Ni, Ca, Fe, Sb, etc.) was inactive with Li, and blocked the aggregation of Sn particles during cycling. However, it sacrificed the capacity itself.

Recently, metal-oxide nanoparticles with different morphologies have been studied intensively for potential applications, such as sensors and magnetic/electronic devices. However, applications to Li-ion cells have been limited.[14−20] Moreover, the correlation between the nanoparticle size and the cycling stability was not systematically studied. Graetz et al. proposed that the size of the Si nanoparticle for Li-ion cells should be <15 nm to improve the cycle-life performance.[21] Herein, we report the critical size of SnO_2 nanoparticle and its effect on the cycling stability.

Experimental Section

SnO_2 nanoparticles with an average size of ∼3, ∼4, and ∼8 nm were synthesized from $SnCl_4$ and triethylenediamine (TEDA: $C_6H_{12}N_2$) as a capping agent using a hydrothermal method. $SnCl_4$ (1 g) was first dissolved in 50 g of distilled water, and 0.5 g of

* Corresponding authors. E-mail: byungwoo@snu.ac.kr (B.P.); jpcho@kumoh.ac.kr (J.C.).
† Seoul National University.
‡ Kumoh National Institute of Technology.

(1) Idota, Y.; Kubota, T.; Matsufuji, A.; Maekawa, Y.; Miyasaka, T. *Science* **1997**, *276*, 1395.
(2) Coutney, I. A.; Dahn, J. R. *J. Electrochem. Soc.* **1997**, *144*, 2045.
(3) Brousse, T.; Retoux, R.; Herterich, U.; Schleich, D. M. *J. Electrochem. Soc.* **1998**, *145*, 1.
(4) Coutney, I. A.; McKinnon, W. R.; Dahn, J. R. *J. Electrochem. Soc.* **1999**, *146*, 59.
(5) Li, N.; Martin, C. R.; Scrosati, B. *Electrochem. Solid-State Lett.* **2000**, *3*, 316.
(6) Retoux, R.; Brousse, T.; Schleich, D. M. *J. Electrochem. Soc.* **1999**, *146*, 2472.
(7) Nam, S. C.; Kim, Y. H.; Cho, W. I.; Cho, B. W.; Chun, H. S.; Yun, K. S. *Electrochem. Solid-State Lett.* **1999**, *2*, 9.
(8) Crosnier, O.; Brousse, T.; Devaux, X.; Fragnaud, P.; Schleich, D. M. *J. Power Sources* **2001**, *94*, 169.
(9) Huggins, R. A.; Boukamp, B. A. U.S. Patent 4,436,796, 1984.
(10) Nazar, L. F.; Goward, G.; Leroux, F.; Duncan, M.; Huang, H.; Kerr, T.; Gaubicher, J. *Int. J. Inorg. Mater.* **2001**, *3*, 191.
(11) Yang, J.; Winter, M.; Besenhard, J. O. *Solid State Ionics* **1996**, *90*, 281.
(12) Tirado, J. L. *Mater. Sci. Eng. R* **2003**, *40*, 103.
(13) Besenhard, J. O.; Yang, J.; Winter, M. *J. Power Sources* **1997**, *68*, 87.
(14) Yin, Y.; Lu, Y.; Sun, Y.; Xia, Y. *Nano Lett.* **2002**, *2*, 427.
(15) Xu, R.; Zeng, H. C. *J. Phys. Chem. B* **2003**, *107*, 12643.
(16) Sun, S.; Murray, C. B.; Weller, D.; Folks, L.; Moser, A. *Science* **2000**, *287*, 1989.
(17) Gerion, D.; Zaitseva, N.; Saw, C.; Casula, M. F.; van Buuren, T.; Galli, G. *Nano Lett.* **2004**, *4*, 597.
(18) Sigman, M. B., Jr.; Ghezelbash, A.; Hanrath, T.; Saunders, A. E.; Lee, F.; Korgel, B. A. *J. Am. Chem. Soc.* **2003**, *125*, 16050.
(19) Alivisatos, A. P. *J. Phys. Chem.* **1996**, *100*, 13226.
(20) Templeton, A. C.; Wuelfing, W. P.; Murray, R. W. *Acc. Chem. Res.* **2000**, *33*, 27.
(21) Graetz, J.; Ahn, C. C.; Yazami, R.; Fultz, B. *Electrochem. Solid-State Lett.* **2003**, *6*, A194.

10.1021/cm048003o CCC: $30.25
Published on Web 05/10/2005

TEDA was then added under magnetic stirring. The mixture was then transferred into a Teflon-lined stainless steel autoclave and maintained at 110, 150, and 200 °C, for approximately 40 h. The TEDA molecules acted as a capping agent, providing the coordinative saturation of dangling bonds on the surface of SnO_2 nanoparticles, and thereby assisted the stabilization of seeds during the initial stage of hydrothermal reaction. Upon increasing the hydrothermal-reaction temperature, seeds were coarsened into larger particle sizes. The sizes of the nanoparticles were easily controlled and reproducible: for instance, 50 g of the ~3 nm-sized nanoparticles was easily reproduced using this hydrothermal reaction.

After cooling to room temperature, precipitates were washed in water and acetone without a size selection process, and dried for 10 h. Electrochemical studies were carried out using coin-type half cells (2016 type) with a Li counter electrode.[22,23] SnO_2 nanoparticle: binder:carbon black in a weight ratio of 3:1:1 was used as a working electrode. The electrolyte was 1 M $LiPF_6$ with ethylene carbonate/diethylene carbonate/ethylmethyl carbonate (EC/DEC/EMC) (30:30:40 vol. %) (Cheil Industries, Korea), and its purity was 99.99% with 0.01 wt. % HF. X-ray diffraction (XRD: M18XHF-SRA, MAC Science) was used for the SnO_2 nanoparticles, before and after cycling. For transmission electron microscopy (TEM: JEM 3000F, JEOL), the as-prepared SnO_2 nanoparticles were dispersed in ethanol and sonicated for 1 h. The cycled electrodes were sonicated in the acetone for 1 h so that only the active particles were obtained from the composite electrodes.

Results and Discussion

Figure 1 shows the XRD patterns of the SnO_2 nanoparticles synthesized at 110, 150, and 200 °C, respectively. All of the diffraction peaks are indexed as SnO_2 with the space group, $P4_2/mnm$ (136) (JCPDS #41-1445), and no impurity peaks are detected. The broad peaks reveal the presence of nanosized SnO_2 crystals. Using the Scherrer equation, the sizes of the SnO_2 nanoparticles synthesized at 110, 150, and 200 °C were estimated to be 3.0 ± 0.1, 4.0 ± 0.1, and 7.7 ± 0.1 nm, respectively, which are consistent with the TEM observations (Figure 2). The TEM images show the same SnO_2 nanoparticles with ~3, ~4, and ~8 nm-size distributions. The lattice fringes of SnO_2 nanoparticles with (110) and (101) planes are also observed in Figure 2.

The cycle-life performances of the SnO_2 nanoparticles are compared in Figure 3. The SnO_2 anodes were cycled at the rate of 60 mA/g (= 0.08 C) for the first cycle, and at a charge rate of 1800 mA/g (= 2.31 C) and a discharge rate of 300 mA/g (= 0.38 C) afterward between 1.2 and 0 V. The ~3 nm-sized SnO_2 nanoparticles showed an initial capacity of 740 mAh/g, which was sustained up to 60 cycles with negligible capacity fading even at a high charge rate. In bulk materials, such capacity retention even at a low charge rate has not been reported. In contrast, the ~4 and ~8 nm-sized anodes showed initial capacity of 636 and 554 mAh/g, and their capacity retentions were ~73% and ~3% after 60 cycles, respectively, as shown in Figure 4a. The most detrimental factor of a SnO_2 anode is the large volume mismatch between Sn and Li_xSn. With the critical size (~3 nm) of the SnO_2 nanoparticles, a superior electrochemical

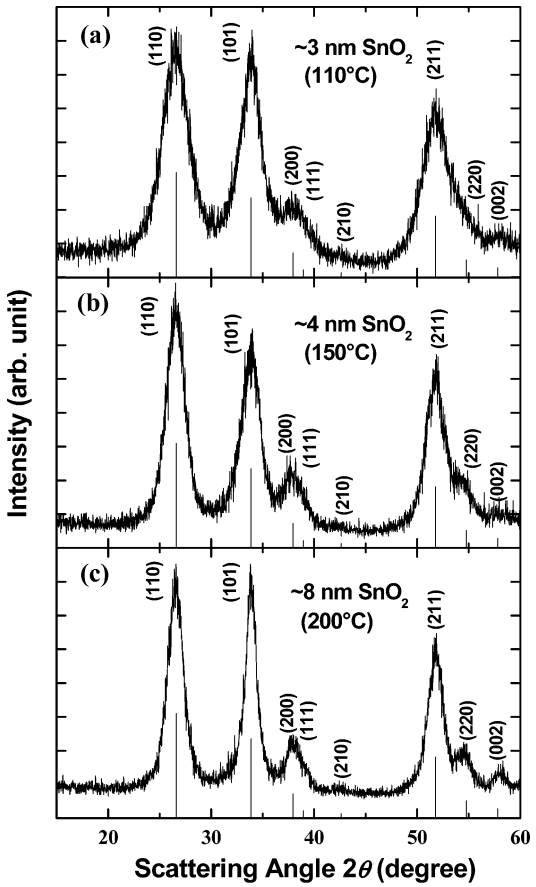

Figure 1. XRD patterns of the SnO_2 nanocrystals before cycling, which were synthesized at (a) 110 °C, (b) 150 °C, and (c) 200 °C. The ideal peak positions and intensities for tetragonal SnO_2 are marked (JCPDS #41-1445).

stability was obtained by a reversible volume change without aggregation of Sn during lithiation/delithiation, which is in contrast to that observed with the ~4 and ~8 nm-sized SnO_2 nanoparticles. Furthermore, the effect of the amounts of carbon black and binder on the cycling behavior was examined. The cyclability of the electrodes with 80 wt. % SnO_2 (~3 nm) was quite similar to those with 60 wt. % SnO_2 at the same C rate, as shown in Figure 4b. It is generally known that more binder and carbon conductor are required to overcome the large volume expansion of the Sn-based electrodes.[24] However, in the case of the well-distributed ~3 nm-sized SnO_2 electrodes, the effect was indistinguishable up to 80 wt. %.

The cycled SnO_2 nanoparticles were examined by XRD and TEM to confirm the origin of the excellent cycling stability of the ~3 nm-sized SnO_2 nanoparticles. After 30 cycles, all of the cells were disassembled and dried in an argon-filled glovebox for 24 h. The dried nanoparticles were sonicated in acetone for 1 h to remove the organic residue. All samples were kept in the vacuum desiccator to minimize the air exposure. Figure 5 shows the XRD patterns of the SnO_2 nanoparticles after 30 cycles. The ~3 nm-sized nanoparticles show SnO_2 crystalline peaks, probably due to the oxidation of small Sn nanoparticles during air exposure for approximately 1 h. It is well known that metal nanoparticles are easily oxidized in air. However, the TEM image

(22) Cho, J.; Kim, Y. J.; Kim, T.-J.; Park, B. *Angew. Chem., Int. Ed.* **2001**, *40*, 3367.
(23) Cho, J.; Kim, Y.-W.; Kim, B.; Lee, J.-G.; Park, B. *Angew. Chem., Int. Ed.* **2003**, *42*, 1618.
(24) Kim, T.-J.; Son, D.; Cho, J.; Park, B.; Yang, H. *Electrochim. Acta* **2004**, *49*, 4405.

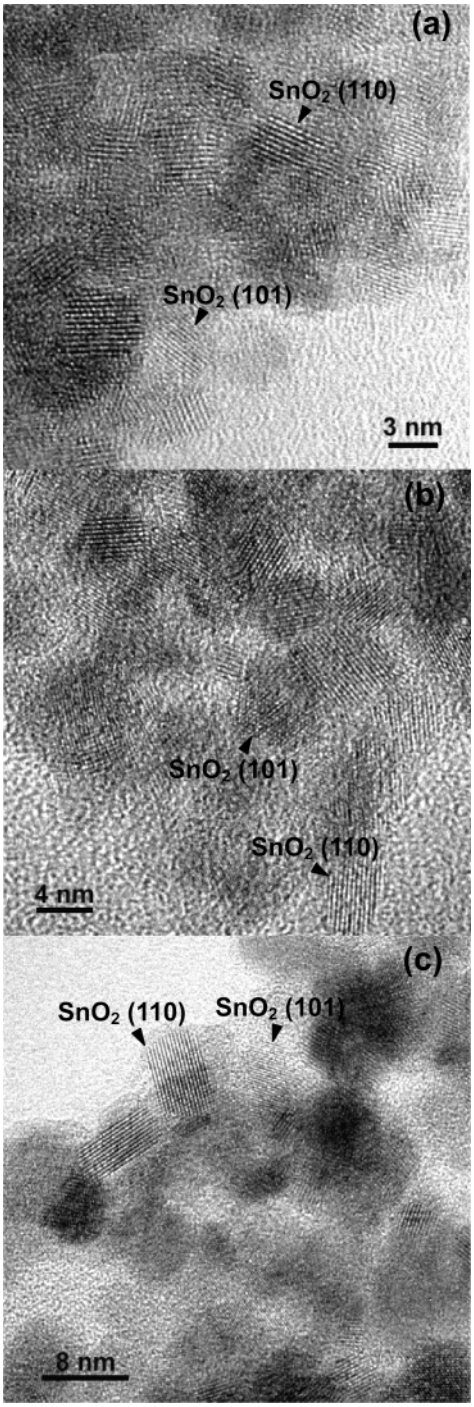

Figure 2. High-resolution TEM images of the SnO_2 nanocrystals before cycling, synthesized at (a) 110 °C, (b) 150 °C, and (c) 200 °C.

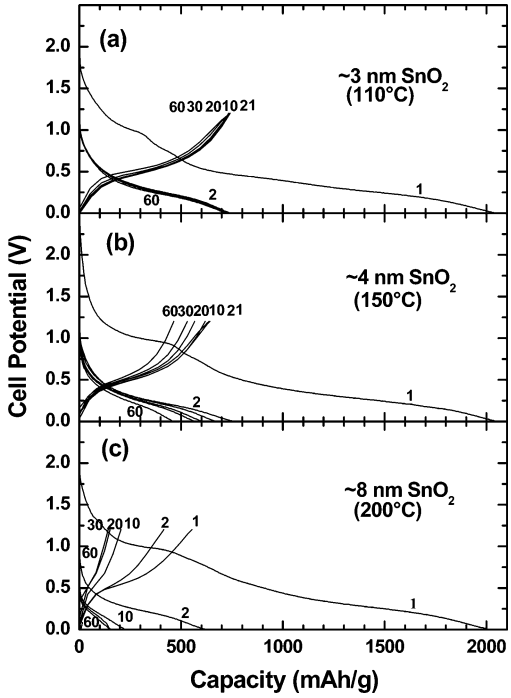

Figure 3. Voltage profiles of the SnO_2 nanoparticles as a function of (a) ~3 nm, (b) ~4 nm, and (c) ~8 nm in coin-type half cells. SnO_2 anodes were cycled at the rate of 60 mA/g (= 0.08 C) for the first cycle, and at the charge rate of 1800 mA/g (= 2.31 C) and the discharge rate of 300 mA/g (= 0.38 C) between 1.2 and 0 V for the remaining cycles.

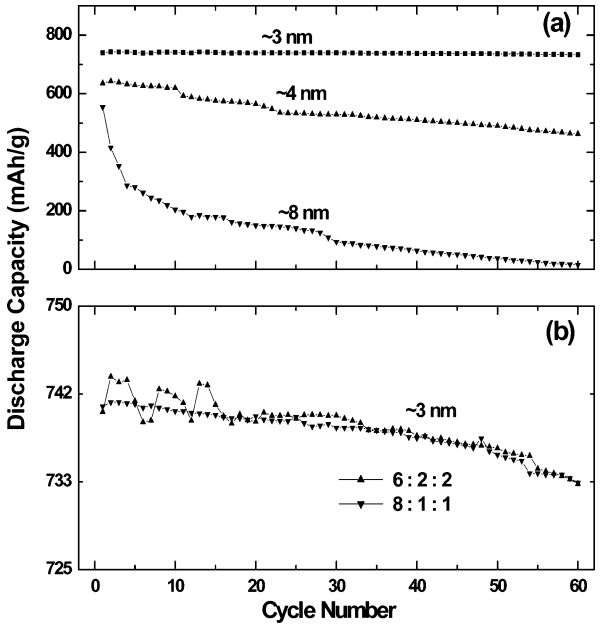

Figure 4. Cycle-life performance of the SnO_2 nanoparticles as a function of (a) size (~3, ~4, and ~8 nm) and (b) electrode composition (SnO_2: binder:carbon black in a weight ratio of 6:2:2 and 8:1:1). The charge cutoff-voltage was 1.2 V.

of the ~3 nm-sized SnO_2 nanoparticles (Figure 6) shows both a few nanometer-sized SnO_2 nanoparticles and tetragonal Sn (*t*-Sn) nanoparticles without aggregation into larger Sn clusters. The lattice fringes of SnO_2 (110) and *t*-Sn (200) planes are shown. The diffraction pattern also confirms SnO_2 and *t*-Sn, as shown in the inset. Tetragonal Sn nanoparticles are observed by TEM as a result of the negligible air exposure (~1 min), as compared to ~1 h in XRD.

The XRD patterns of the ~4 nm-sized nanoparticles (Figure 5b) show cubic Sn (*c*-Sn) crystalline peaks. In the case of the ~4 nm-sized SnO_2 nanoparticles, the Sn nanoparticles were more stable in air as compared to the ~3 nm-sized nanoparticles. The presence of *c*-Sn without oxidation was also confirmed by TEM. The XRD patterns of the ~8 nm-sized particles show a *t*-Sn phase. The TEM image of the ~8 nm-sized SnO_2 nanoparticle (Figure 7a) shows *t*-Sn nanoparticles with various sizes. Even large Sn clusters over ~100 nm were observed. The selected area diffraction (SAD) pattern is indexed to *t*-Sn. In the case of the ~8 nm-sized SnO_2 nanoparticles (and the ~4 nm-sized ones), the Sn particles were quite stable in air. Sn nanoparticles over a critical size appear to aggregate into larger stable

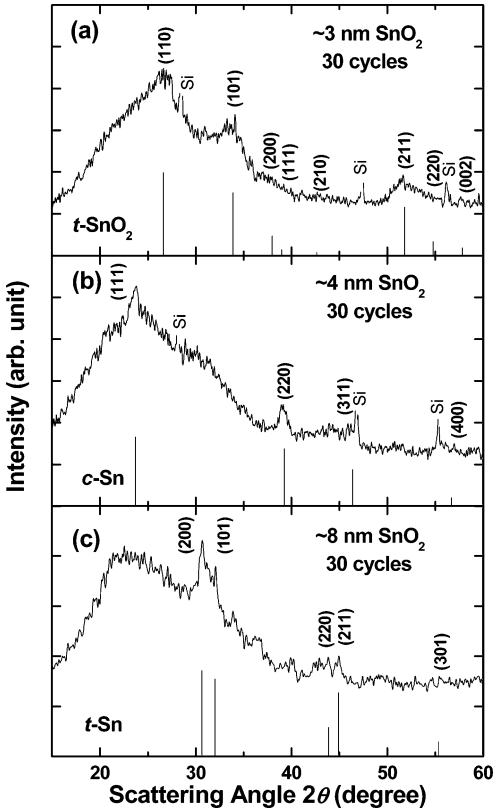

Figure 5. XRD patterns of the SnO_2 nanoparticles at 1.2 V as a function of size, (a) ~3 nm, (b) ~4 nm, and (c) ~8 nm, after 30 cycles between 0 and 1.2 V. The diffraction patterns are indexed to tetragonal SnO_2, cubic Sn, and tetragonal Sn in (a), (b), and (c), respectively. The ideal peak positions and intensities are marked for tetragonal SnO_2 (JCPDS #41-1445), cubic Sn (#05-0390), and tetragonal Sn (#04-0673), respectively.

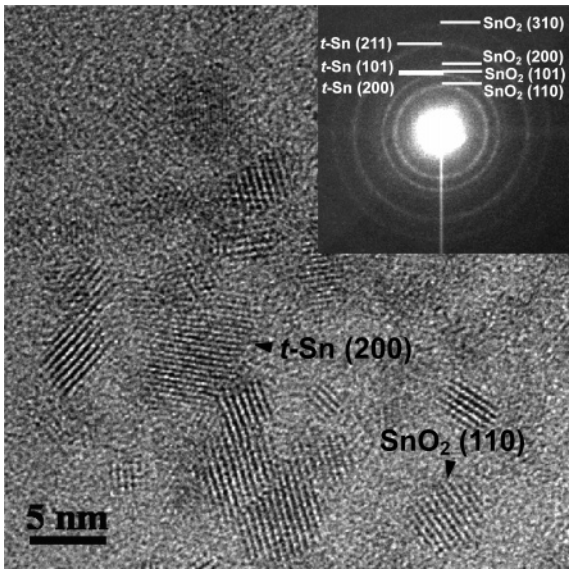

Figure 6. High-resolution TEM image of ~3 nm-sized SnO_2 nanocrystals after 30 cycles. Aggregation into the larger Sn particles is not shown. The inset image is a diffraction pattern showing SnO_2 and tetragonal Sn.

Sn clusters during cycling. Figure 7b shows a magnified image of the circled region in Figure 7a, showing the core-shell structure of the Sn clusters. A ~30 nm-sized Sn cluster is surrounded by a few nanometer-sized Sn particles. Once a large Sn cluster is formed, it appears to be favorable for a larger Sn cluster to form at the expense of smaller ones. Therefore, as shown in Figure 7b, the larger Sn cluster

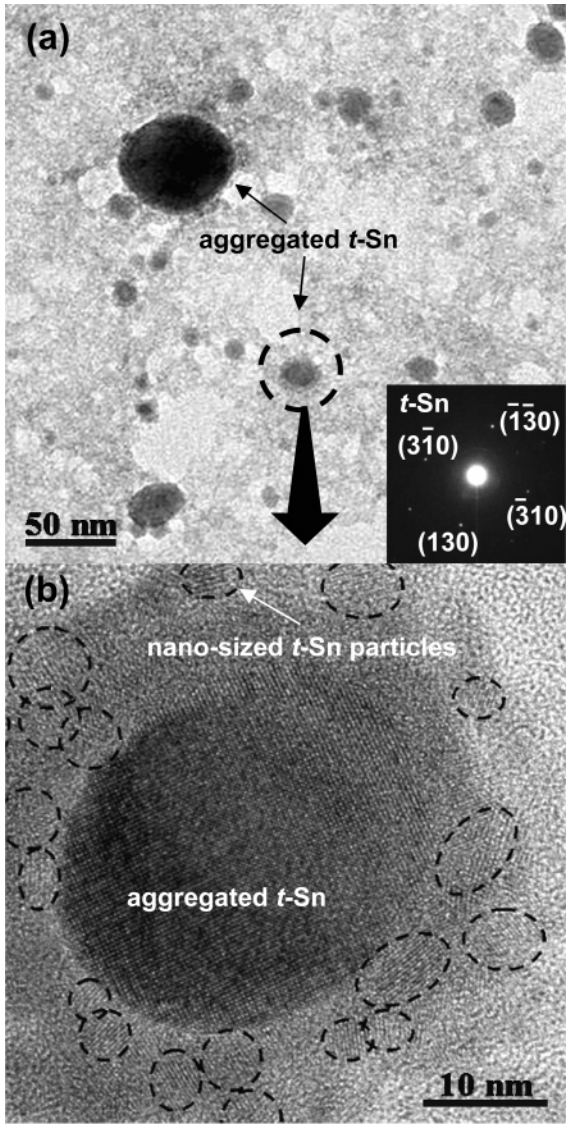

Figure 7. (a) High-resolution TEM image of ~8 nm-sized SnO_2 nanocrystals after 30 cycles. Aggregation into larger clusters is shown. The inset image is a SAD pattern along the [001] zone axis showing tetragonal Sn. (b) Magnified image of the circled region in (a). A few nanosized Sn nanoparticles aggregate into the larger Sn clusters, to minimize the surface energy among the particles.

assembles smaller ones to minimize the surface energy among the particles. These large Sn particles may not maintain their integrity due to the large volume change during cycling, resulting in poor capacity retention. The ~3 nm sized SnO_2 nanoparticles did not aggregate after cycles, yielding excellent capacity retention. On the other hand, both ~4 and ~8 nm-sized samples exhibited apparent capacity decay, and the latter electrode (having 97% capacity decay after 60 cycles) was clearly separated from the Cu current collector.

Conclusions

The critical size of SnO_2 nanoparticles with an average size of ~3 nm showed an initial charge capacity of 740 mAh/g, with negligible capacity fading after 60 cycles even at a high charge rate. The principal reason of this superior electrochemical property is that the Sn nanoparticles undergo a reversible volume change without aggregation into larger Sn clusters during cycling, which is confirmed by XRD

and TEM. SnO_2 nanoparticles are one of the most promising candidates for replacing the conventional graphite anode in Li-ion cells. However, it has a relatively large irreversible capacity as compared to the theoretical value. The large irreversible capacity of the nanosized SnO_2 electrode is probably due to the severe side reaction of the enlarged surface area with the electrolyte.[25] This large irreversible capacity may be minimized by the surface coating, additives, or other treatments that prohibit the side reaction with electrolyte. Also, mixing SnO_2 with nano-sized metal oxides may facilitate Li_2O matrix reversibly.[26] Further studies are currently underway to resolve this irreversible capacity problem in the nano Sn-based anode materials.

Acknowledgment. This work was supported by KOSEF through the Research Center for Energy Conversion and Storage at Seoul National University, by the National R&D Program of the Ministry of Science and Technology, by the University IT Research Center Project, and by the Basic Research Program (R01-2004-000-10173-0) of KOSEF.

CM048003O

(25) Aurbach, D.; Nimberger, A.; Markovsky, B.; Levi, E.; Sominsky, E.; Gedanken, A. *Chem. Mater*. **2002**, *14*, 4155.

(26) Poizot, P.; Laruelle, S.; Grugeon, S.; Dupont, L.; Tarascon, J.-M. *Nature* **2000**, *407*, 496.